AIAA 81-2048R

Assessment of Inflow Control Structure Effectiveness and Design System Development

A. A. Peracchio*
Pratt & Whitney Aircraft Group, East Hartford, Connecticut

Use of inflow control structures during static testing of fans is shown to minimize inflow distortions, thereby simulating the fan's inflight flowfield and noise generating mechanisms. Results of acoustic testing of a Pratt and Whitney Aircraft JT9D engine with and without an inflow control structure are presented and compared, after projection to flight, with measured flight levels from a JT9D equipped Boeing 747 aircraft. The use of an inflow control structure is shown to significantly reduce the blade passage frequency tone and to improve agreement between static data projected to flight and the flight data. The inflow control structure had a negligible effect on the tone at twice blade passage frequency. A design procedure is also presented that prescribes the inflow control structure shape, size, and detailed construction.

Nomenclature

BPF = blade passage frequency, Hz
d_{ICS} = maximum characteristic dimension of inflow control structure material (e.g., honeycomb cell size), m
ICS = inflow control structure
k_1^* = wavenumber, m^{-1}
k_{2L} = wavenumber, m^{-1}
k_{2U} = wavenumber, m^{-1}
k_{3L} = wavenumber, m^{-1}
k_{3U} = wavenumber, m^{-1}
K_H = honeycomb resistance
K_p = perforated plate resistance
L_{AF} = characteristic length scale of turbulence flight case, m
L_{AS} = characteristic length scale of turbulence static case, m
L_{ICS} = characteristic length scale of turbulence behind inflow control structure, m
l_{IF} = final contraction ratio (inflow control structure to fan face)
l_{II} = initial contraction ratio
l_{IS} = static contraction ratio
l/d = honeycomb length-to-diameter ratio
l_p = perforated plate thickness, m
M_{ICS} = maximum Mach number incident to inflow control structure
$N_1/\sqrt{\theta}$ = corrected fan rotor rotational speed, rev/s
N_F = turbulence field characteristic, defined in step 20 of design procedure, m/s^2
Re = Reynolds number of honeycomb cell
R_{ICS} = nominal radius of inflow control structure, m
R_0 = inlet radius at fan face, m
U_{1A} = streamwise velocity deficit in wake before contraction, m/s
U_{2A} = maximum azimuthal velocity in vortex before contraction, m/s
U_A = maximum wind velocity in test window, m/s
$\sqrt{\overline{u_{AF}^2}}$ = root-mean-square value of turbulent velocity in-flight, m/s
$\sqrt{\overline{u_{AS}^2}}$ = root-mean-square value of turbulent velocity statically, m/s
U_{ICS} = throughflow design speed at inflow control structure, m/s
U_{REF} = static reference wind speed, m/s
U_0 = inlet velocity at lowest speed of interest along engine operating line, m/s
z = engine centerline height above ground during static test, m
z_0 = roughness scale, m
z_{REF} = reference height, m
α_H = flow angle ratio—honeycomb
α_p = flow angle ratio—perforated plate
γ_F = turbulence field characteristics defined in step 20 of design procedure, m^{-1}
γ' = blade relative inflow angle, deg
θ = ambient static temperature = °K/288 °K
λ_{min} = minimum sensitive transverse scale, m
$(\lambda_{min})_{ICS}$ = minimum sensitive transverse scale at inflow control structure, m
ν = kinematic viscosity of air, m^2/s
σ_p = open area ratio for perforated plate
2BPF = twice blade passage frequency, Hz

Introduction

REDUCTION of aircraft engine noise levels is a continuing process which has resulted in significant noise reduction since the advent of the original commercial jet aircraft in the early 1950s. Engine noise reduction features are usually verified by means of static or flight testing. Since the cost of flight testing is much greater than that of static testing, use of the latter technique results in significantly lower costs being accrued to the development of engine noise reduction features. As such, the use of static testing techniques should be fully exploited.

It has been noted by various observers that the noise produced by the fan of some turbofan engines operating statically on the test stand is greater than that produced when the engine is operating under flight conditions. This may be a result of both fan blade passing tone and broadband levels being contaminated by extraneous noise sources present during static testing. As a consequence, predictions of flight noise levels using static data are high. Depending on the engine type, it is also possible that flight noise sources cannot be identified from noise data acquired in static tests, and therefore noise reduction techniques cannot be evaluated on the test stand in the presence of contaminating extraneous noise. The source of the extraneous noise is the distorted fan inflow that exists during static testing, but not in flight. In order to reduce or eliminate this flow distortion, inflow

Presented as Paper 81-2048 at the AIAA 7th Aeroacoustics Conference, Palo Alto, Calif., Oct. 5-7, 1981; submitted Oct. 15, 1981; revision received Feb. 16, 1982.

*Senior Project Engineer, Commercial Products Division. Member AIAA.

control structures (ICS) have been used during static testing and found to be effective. In this paper, it is shown that inflow control structures used during static testing of fans minimize inflow distortions, thereby simulating the fan's in-flight flowfield and noise generating mechanisms. Results of acoustic testing of a Pratt and Whitney Aircraft JT9D engine with and without an inflow control structure are presented and compared, after projection to flight, with measured flight levels from a JT9D equipped Boeing 747 aircraft.

Assessment of Inflow Control Structure Effectiveness

Description of Test Programs

The static data were obtained from a JT9D hardwalled engine tested at Pratt and Whitney Aircraft's outdoor acoustic test stand with and without an inflow control structure designed by Pratt and Whitney Aircraft. The engine with the inflow control structure is shown in Fig. 1. The flight data were obtained from flyovers of a Boeing 747 aircraft equipped with four hardwalled JT9D engines of the same model as that used in the static tests. Comparisons to flight were made for static data obtained with and without the inflow control structure to assess the improvements afforded by use of the inflow control structure. The comparisons were made for blade passage frequency and twice blade passage frequency from data obtained from one-third octave band spectra. Flyover data were available for four flight conditions: approach with 30-deg flap setting; approach with 25-deg flap setting, takeoff, and cutback. The flight data were recorded by pole microphones located at a height of 1.22 m over the runway surface. Details of the flight path, etc., are given in Table 1.

The flight acoustic data have been corrected as follows.

1) Raw data are corrected to 77 deg, 70% relative humidity Federal Aviation Agency (FAA) day.

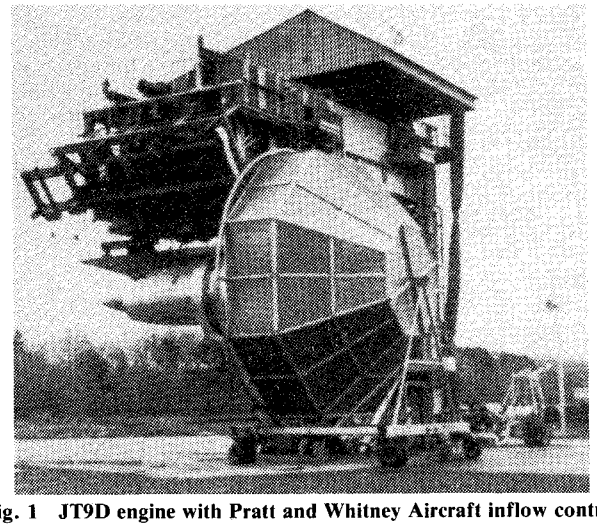

Fig. 1 JT9D engine with Pratt and Whitney Aircraft inflow control structure.

2) Data are corrected to the flight path cited above.

3) Microphone incidence angle correction was applied to the data.

4) The data were time-averaged over 0.5-s intervals. Values of the time-averaged data for the static measurement angles used in the assessment were obtained by interpolation knowing the relationship between angle and flyover time.

Static data, obtained from pole microphones over trap rock arranged along a 150 ft radius, at a height equal to the engine centerline were also corrected to a Federal Aviation Agency day. Tone levels from one-third octave band spectra were then projected to simulate the flight case and compared to the tones from one-third octave band spectra obtained from the flyover data to assess the inflow control structure effectiveness. Reference 1 describes the procedure used to project the statically obtained tone levels to flight. The flyover comparisons are plotted vs measurement angle. For a given measurement angle and flight-corrected fan speed, the tone level was obtained by interpolating the sound pressure level in the one-third octave bands containing the fan tones over speed and angle. Observations of narrow-band spectra for a range of angles and engine operating conditions show the fan tone frequency one-third octave band SPL levels to be set by the fan tones.

The tone levels were projected to flight, accounting for spherical divergence, air attenuation, convective amplification, doppler effects, and ground reflection effects.

Comparison of Static Data Projected to Flight and Flight Data

Static data obtained with and without an inflow control structure were projected to flight and compared to flyover data. Comparisons for blade passage frequency and twice blade passage frequency tone levels were made for the conditions shown in Table 1. Reference 1 contains all the comparisons. For purposes of this paper, selected samples will be shown and the significant conclusions discussed.

Consider first the tone at twice blade passage frequency. Figure 2 shows the comparison for the approach condition corresponding to a 30-deg flap setting. This is typical of the comparisons at other operating conditions. As can be seen for the JT9D engine, the use of an inflow control structure had a small effect on the twice blade passage frequency tone. This was also the case for the three other conditions considered and indicates that rotor-inflow distortion during static testing without an inflow control structure is not a dominant source of twice blade passage frequency tone noise and further indicates that the inflow control structure does not significantly attenuate or alter the directivity pattern of the twice blade passage frequency tone. Figure 2 also shows flyover data for twice blade passage frequency. The predictions based on static data, when compared to flight data, tend to be high in the forward angles and low in the rear angles for this case. For the other approach and cutback conditions the predictions are also higher than the measured for the forward angles and lower for the aft angles. For the takeoff case, the predictions based on static data are generally greater than the measured

Table 1 Flight-path information

Flight condition	Nominal corrected speed $N_1/\sqrt{\theta}$, rpm	Altitude at overhead, m	Flight velocity, m/s	Climb angle, deg	Pitch of aircraft, deg	Nacelle angle relative to aircraft, deg
Approach 30-deg flap	2296	113	80	−3	0.8	2.3
Approach 25-deg flap	2327	113	80	−3	0.8	2.3
Takeoff	3270	244	100	4.97	14.2	2.3
Cutback	3008	244	100	2.29	11.0	2.3

flight data for all angles. These comparisons suggest that a possible reason for the discrepancy is that the convective amplification correction may be too high in the forward quadrant and too low in the aft. A reduction in exponent from the value of four commonly used would result in improved agreement between the predictions and the measured data. The corrections used to project static data to flight are consistent with the current state-of-the-art. It is difficult to pinpoint errors in any one of these corrections (i.e., convective amplification) as being totally responsible for the observed differences between predicted and measured flyover data. Other effects not included in the projection of static data to flight could also contribute to the discrepancies. These include 1) long distance propagation in the atmosphere, i.e., sound is scattered by turbulence in the atmosphere, an effect which is currently not included in the corrections; 2) nonlinear sound propagation effects which become significant at large propagation distances; 3) refraction of sound by velocity and temperature gradients in the atmosphere, although they can be partially included by use of a layered atmosphere; and 4) reflection and diffraction effects caused by an aircraft's wings, fuselage, and wakes.

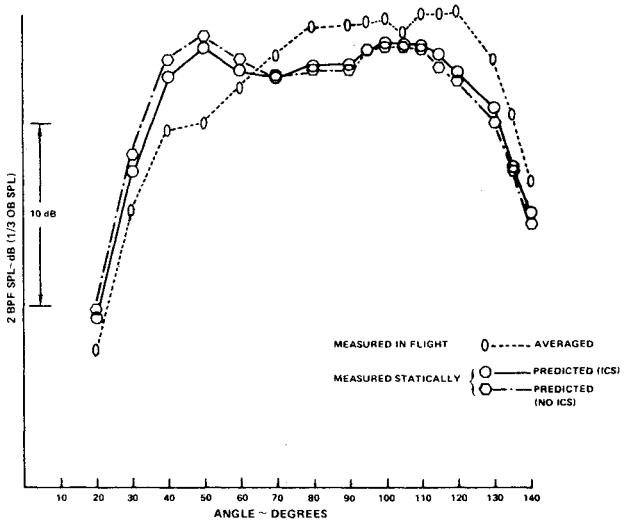

Fig. 2 Comparison of twice blade passage frequency tone levels (based on static data) with measured flyover tone levels; approach 30-deg flap.

Consideration of the blade passage frequency tone showed a significant impact on the blade passage frequency tone of the static data when using an inflow control structure. In addition, agreement between static data projected to flight and flight data was greatly improved by use of an inflow control structure. These results can be seen from the plots of the blade passage frequency tone vs angle shown in Figs. 3-6 for the conditions of Table 1.

The variability in the static data is shown by the bars on the figures. These bars were derived as follows. The flyover noise prediction at a particular angle is based on a curve which is spline fit, as a function of corrected speed, through measured static data at that angle, rather than on the static data points themselves. The scatter of the measured data about this curve is a source of variability in the prediction. An indication of the prediction variability within the range of applicable operating speeds and at each angle was obtained from the standard deviation of the SPL differences between the various data points and the spline fit used in the prediction. The degree of variability in the measured flyover data was estimated from a comparison of blade passage frequency vs angle curves for two similar flight conditions.

For each of the conditions examined, an angle average of the measured flight mean blade passage frequency tone minus the predicted value based on the averaged measured static data projected to flight was carried out to quantify the extent to which 1) the use of an inflow control structure improved prediction accuracy, and 2) the use of an inflow control structure reduced the scatter in the difference between measured and predicted noise levels.

Table 2 shows the results of the angle averaging. Considering first the analyses for each power setting, it is clear that differences between the predicted and measured data are reduced with the use of an inflow control structure. In fact, if differences are averaged for all power settings and angles, it can be seen that without an inflow control structure, blade passage frequency is predicted 3.9 dB higher than measured. Use of an inflow control structure results in only a 0.8-dB overprediction, a significant improvement. If the standard deviations in Table 2 are studied, it can be seen that the use of an inflow control structure does not significantly alter the scatter of the predictions relative to the data.

Based on the blade passage frequency comparisons of Table 2, data obtained statically from a JT9D engine with the Pratt and Whitney Aircraft inflow control structure installed and projected to flight, on the average, gave predictions that were 0.8 ± 1.9 dB higher than measured. Similar data projections

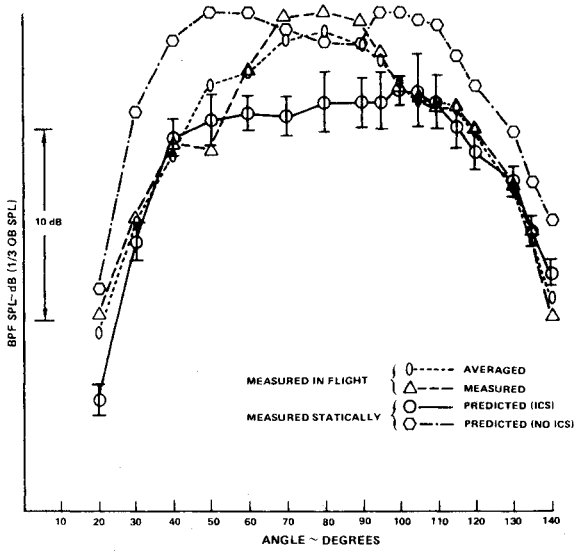

Fig. 3 Comparison of predicted flight BPF tone levels (based on static data) with measured flyover tone levels; approach 30-deg flap.

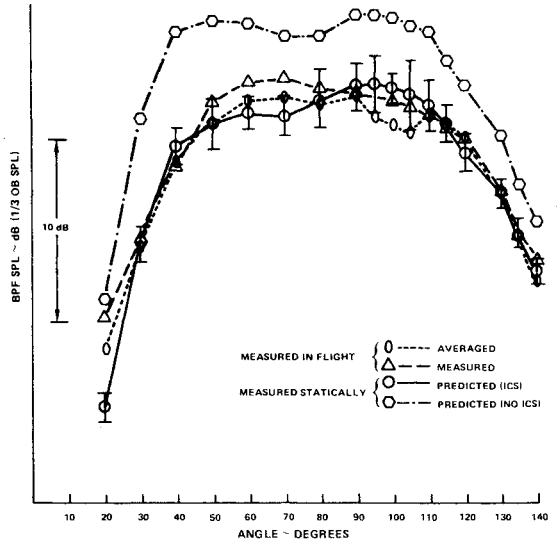

Fig. 4 Comparison of predicted flyover BPF tone levels (based on static data) with measured flyover tone levels; approach 25-deg flap.

without an inflow control structure gave predictions that were 3.9 ± 1.8 dB higher than measured.

Further evaluations of the Pratt and Whitney Aircraft inflow control structure are reported in Ref. 2. Comparisons are made at the spectral level for three angles using data for approach and takeoff power (see Figs. 21-24 of Ref. 2). As is evident, there is very good agreement between the flyover data and the static data projected to flight. In addition, since Federal Aviation Agency noise certification procedures require assessment of noise levels in terms of perceived noise levels (PNL), perceived noise level time histories are also compared in Fig. 25 of Ref. 2. Again, very good agreement results.

In Ref. 3 analysis of fan blade mounted transducer (BMT) data shows that use of an inflow control structure greatly reduces the inflow distortion at the fan face. Further, with the exception of the flow in the fan duct boundary layer, use of an inflow control structure produces BMT data that closely approximate those in flight.

From the above discussions, the following observations can be made.

The use of an inflow control structure in static fan noise testing of high bypass ratio engines, combined with a comprehensive static-to-flight projection technique, provides an improved method for obtaining predictions of flight fan noise levels using static data. Even with the use of an ICS, differences still exist between static data projected to flight and flight data, pointing to the need for further refinements in the methodology used to project static data to flight.

The inflow control structure effectiveness has been demonstrated for the JT9D-7 engine type. Other high bypass ratio engines with different fan noise characteristics may show different acoustic results, and further evaluation using other engine data would be beneficial in further verifying inflow control structure effectiveness.

Inflow Control Structure Design System

Inflow Control Structure Design Target

The atmospheric turbulence intensities and length scales that exist during static testing and in-flight can be obtained from the results of Ref. 4 as a function of altitude above the ground, mean wind velocity, surface roughness, and atmospheric stability.

Analytical studies of rotor-turbulence interactions show that the mechanism is dominated by distortion elements within a small range of transverse scales. For typical turbulence energy distributions encountered in the atmosphere, this range covers about one decade and is centered around a transverse scale in the order of 30% of the rotor blade spacing at the blade tip. For a given turbulence variance, maximum sound power levels are achieved at transverse integral scales in the order of 25% of the rotor blade spacing at the blade tip. For a JT9D fan this is about 4.1 cm and for the JT15D fan it is about 1.3 cm.

Table 2 Comparison of averaged measured minus predicted values of BPF tone for cases with and without an ICS[a]

Flight condition	No ICS $(BPF_{ma} - BPF_{PNI})^a$ dB	With ICS $(BPF_{ma} - BPF_{PI})^a$ dB
Approach 30 deg flap	−3 ±1.7	1.2±1.6
Approach 25 deg flap	−4.5±1.4	−0.1±1.4
Takeoff	−3.2±1.5	−1.8±2.3
Cutback	−5.0±2.7	−2.6±2.3
Average over all angles and power settings	−3.9±1.8	−0.8±1.9

[a] $(\ )_a$ = average over measurement angles; BPF_{ma} = BPF tone level measured in flight; BPF_{PNI} = BPF tone level projected to flight from static data, no ICS; BPF_{PI} = BPF tone level projected to flight from static data, with ICS.

Based on the atmospheric turbulence model and the analytical contraction models from Ref. 4, the prediction of rotor-turbulence interaction noise statically and in-flight for JT9D and JT15D sized engines shows that tone levels at approach power are on the order of 30 dB higher under static conditions than they are in-flight. This points out the importance of suppressing the rotor-atmospheric turbulence interaction during static testing. Since the rotor-turbulence interaction tone noise level is so low in-flight, designing the inflow control structure to achieve flight levels of turbulence during static testing would provide a conservative inflow control structure design.

In considering steady distortions, it was shown in Ref. 5 that the transverse velocity component of steady or quasisteady distortions is not suppressed by flow contractions. Since distortions with significant components of transverse velocity can be generated by flow over the ground plane (e.g., ground vortex), and, it is conjectured by flow ove. the stand structure, it is important to suppress these velocities with an inflow control structure. Wakes with axial velocity deficits are also generated by the test stand structure, and although flow contraction tends to reduce these distortions, an inflow control structure design should also suppress steady axial velocity distortions. In order to provide a design goal, it is necessary to specify the level to which the inflow control structure should suppress the steady distortions. Based on the studies described above, it was shown that in-flight, levels of the turbulence involved in fan noise generation were so low that the resulting fan tone noise was about 30 dB (based on an analysis bandwidth equal to 1% of blade passage frequency) below that generated under static conditions. Furthermore, experimental data show that these static levels are about 5-10 dB higher than typical fan tones generated with the turbulence suppressed. Thus the in-flight rotor-turbulence interaction mechanism is on the order of 20 dB below the fan-generated noise levels. The in-flight turbulence level therefore provides a conservative target at which to aim the inflow control structure design. Accordingly, for both turbulence and steady inflow distortion suppression, the goal of the inflow control structure design will be to simulate in-flight turbulence levels.

Overview of Inflow Control Structure Design System

The inflow control structure design system is based on the analytical models and experimental data described in Refs. 4 and 5. The system provides, as an output, the inflow control structure radius and covering material details. Two designs

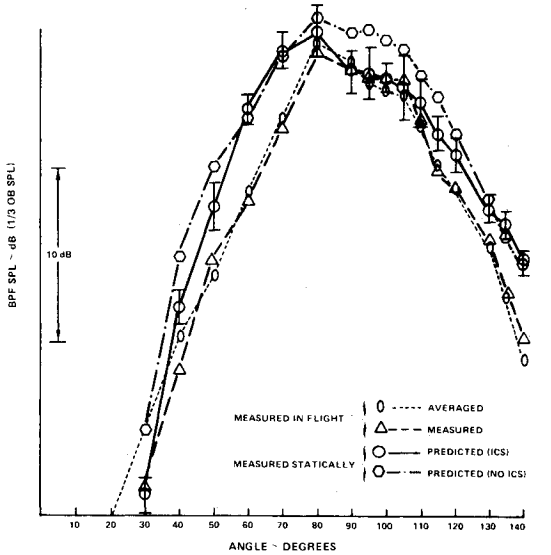

Fig. 5 Comparison of predicted flight BPF tone levels (based on static data) with measured flyover tone levels; takeoff.

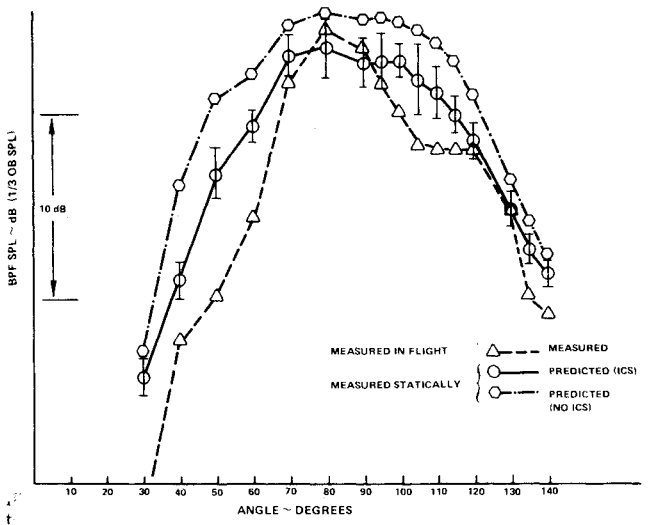

Fig. 6 Comparison of predicted flyover BPF tone levels (based on static data) with measured flyover tone levels; cutback.

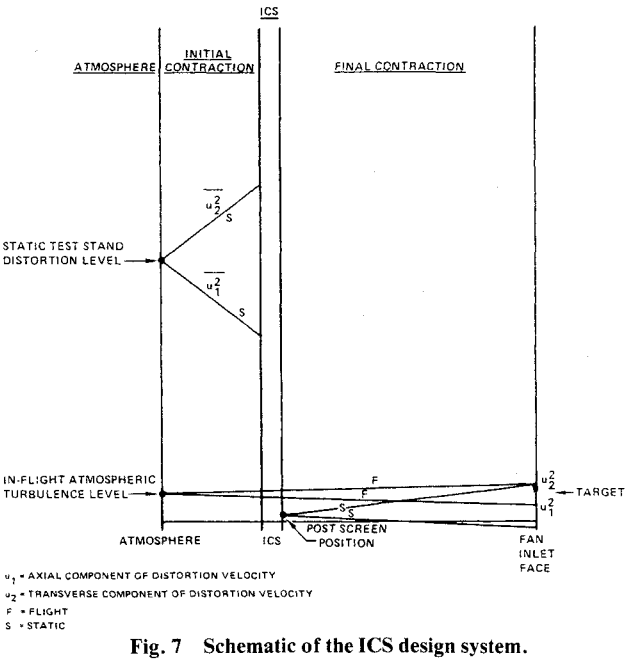

Fig. 7 Schematic of the ICS design system.

are defined, one based on suppression of atmosphere turbulence and the other based on suppression of inflow distortion. The more conservative design is selected for application to engine testing. The details of the inflow control structure design system and its development are given in Ref. 5. Only the design system and a brief description of its major elements will be given here.

The major elements of the design systems consist of models for 1) the turbulence in the atmosphere; 2) the effects of contraction on axial and transverse velocity disturbances; and 3) the effects of inflow control structure covering (screening or perforated plate and honeycomb) on axial and transverse velocity disturbances.

Figure 7 shows in schematic form the inflow control structure design system. The atmospheric turbulence model is described in Ref. 4. The contraction effects are accounted for by using a model based on the work of Batchelor, Proudman, Ribner-Tucker, and Prandtl combined with experimental results as described in Ref. 5.

The effect of honeycomb and perforated plate on the axial and transverse velocity components is based on experimental data and the analytical model of Taylor and Batchelor, and is also described in Ref. 5. The target velocity component level (i.e., the in-flight level) is shown in Fig. 7. The design procedure is structured to yield an inflow control structure configuration whose steady and unsteady velocity distortions are less than or equal to the target value as shown by the lines marked by an F.

Inflow Control Structure Design System

Development of the system presented below for the design of inflow control structures is described in detail in Ref. 5. Only the step-by-step procedure is given here. Two design procedures are given, one that results in an inflow control structure design for suppression of turbulence to calculated in-flight turbulence levels and the other that results in a design for suppression of steady distortions to calculated in-flight turbulence levels. The most conservative design is then selected for construction. Note that Honeycomb is used to remove primarily the azimuthal velocity components of inflow distortion whereas perforated plate reduces predominantly the streamwise velocity component of the inflow distortion.

General Information

1) Determine inlet velocity at fan face at lowest operating condition, U_0.

2) Determine maximum ambient wind velocity in test window, U_A.

3) Compute design speed at inflow control structure, U_{ICS},

$$U_{\mathrm{ICS}} = 1.5\, U_A$$

4) Determine inlet radius, R_0.

5) Compute nominal radius of inflow control structure, R_{ICS},

$$R_{\mathrm{ICS}} = R_0\sqrt{U_0/2U_{\mathrm{ICS}}}$$

6) Determine fan rotor blade number, B.

7) Compute minimum sensitive transverse scale, $\lambda_{\min}$,

$$\lambda_{\min} = \pi R_0/5B$$

8) Compute final contraction ratio (inflow control structure to inlet), I_{IF},

$$I_{IF} = U_0/U_{\mathrm{ICS}}$$

(Note: Initial contraction ratio, from atmosphere to inflow control structure, I_{II}, is equal to 1.5 by design.)

9) Compute minimum sensitive transverse scale at inflow control structure, $(\lambda_{\min})_{\mathrm{ICS}}$,

$$(\lambda_{\min})_{\mathrm{ICS}} = I_{IF}^{1/2}\lambda_{\min}$$

10) Compute characteristic detail dimension of inflow control structure material, d_{ICS}(e.g., Honeycomb cell size),

$$d_{\mathrm{ICS}} = 0[\,(\lambda_{\min})_{\mathrm{ICS}}/10]$$

11) Compute Reynolds number of honeycomb cell, Re,

$$\mathrm{Re} = [\,U_{\mathrm{ICS}} d_{\mathrm{ICS}}/\nu]$$

Atmospheric Turbulence Design

12) Determine engine height, z; roughness scale, z_0 (see Fig. 8); static reference height (engine height), z_{REF}; static reference speed (maximum speed in test wind window), U_{REF}.

13) Compute rms value of turbulent velocity in capture stream tube during static operation, $\sqrt{u_{AS}^2}$,

$$\sqrt{u_{AS}^2} = \frac{0.464 R_0^{1/3} U_{\mathrm{REF}}^{5/6} U_0^{1/6} z^{-1/3}}{[\ln(z/z_0)]^{1/6}\,[\ln(z_{\mathrm{REF}}/z_0)]^{5/6}}$$

14) Compute static contraction ratio, l_{IS},

$$l_{IS} = U_0/U_A$$

15) Compute characteristic length scale of turbulence in capture stream tube during static operation, L_{AS},

$$L_{AS} = 0.355 R_0 l_{IS}^{1/2}$$

16) Determine, for flight operation, engine height, z; roughness scale, z_0 (Fig. 8); flight reference height, z_{REF}; flight reference wind speed, U_{REF}.

17) Compute rms value of turbulent velocity in capture stream tube in flight, $\sqrt{\overline{u_{AF}^2}}$,

$$\sqrt{\overline{u_{AF}^2}} = \frac{0.464 R_0^{1/3} U_{REF} z^{-1/3}}{[\ln(z/z_0)]^{1/6} [\ln(z_{REF}/z_0)]^{5/6}}$$

18) Compute characteristic length scale of turbulence in capture stream tube in-flight, L_{AF},

$$L_{AF} = 0.355 R_0$$

19) Compute limits of sensitive wavenumber ranges, k_I^*, k_{2U}, k_{2L}, k_{3U}, k_{3L},

$$k_I^* = B/R_0 \qquad k_{2U} = k_{3U} = 10B/R_0 \qquad k_{2L} = k_{3L} = B/2R_0$$

20) Compute in-flight turbulence field characteristics, N_F, γ_F,

$$N_F = 2\overline{u_{AF}^2}/\pi^2 L_{AF} \qquad \gamma_F = 1/L_{AF}$$

21) Determine blade relative inflow angle at tip, γ'.

22) Compute characteristic length scale of turbulence behind inflow control structure, L_{ICS},

$$L_{ICS} = \frac{4}{3}\frac{L_{AS}}{l_{II}^{1/2}} \qquad \text{if } L_{ICS} > l$$

$$= L_{AS} \qquad \text{otherwise}$$

23) Compute the parameters p and s,

$$p = \frac{k_{2L}^2 L_{ICS}^2}{l_{IF}} \qquad s = p + 1$$

24) Compute maximum value of flow angle ratio product, $\alpha_p \alpha_H$

$$\alpha_p \alpha_H = \left[\frac{32\pi N_F L_{AS}}{l_{IF} l_{II}^{1/2} u_{AS}^2} \times \frac{s(k_{3U} - k_{3L}) k_I^*}{\{4(k_{2L}^2 + \gamma_F^2) + (k_{3U} + k_{3L})^2\}^3} \times \frac{(4k_{2L}^2 \sin^2\gamma' + [k_{3U} + k_{3L}]^2)}{1 + p/2 + (s\sqrt{p}/4)[\sin^{-1}(1 - 2/S) - \pi/2]} \right]^{1/2}$$

25) Solve the equation for perforated plate (gauze) flow angle ratio, α_p,

$$\frac{2\alpha_p^3 + \alpha_p^2 - 1.21\alpha_p}{\alpha_p^3 + 1.21} = 0.866 \alpha_p \alpha_H l_{II}^{2/3} \times \left\{ \frac{\alpha_p + \alpha_p \alpha_H - 0.201 Re^{-1/4} \alpha_p [\ln \alpha_p \alpha_H - \ln \alpha_p]}{\alpha_p + \alpha_p \alpha_H (1 + 0.201 Re^{-1/4} [\ln \alpha_p \alpha_H - \ln \alpha_p])} \right\}$$

26) Compute resistance of perforated plate (gauze), K_p,

$$K_p = 1.21 \alpha_p^{-2} - 1$$

27) Compute flow angle ratio of honeycomb, α_H,

$$\alpha_H = \alpha_p \alpha_H / \alpha_p$$

28) Compute resistance of honeycomb, K_H,

$$K_H = -0.201 Re^{-1/4} \ln \alpha_H$$

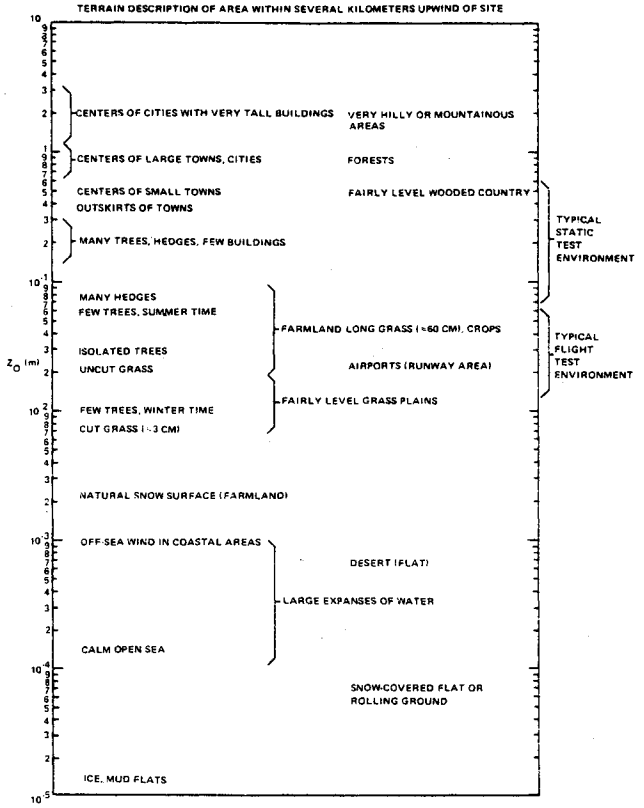

Fig. 8 Values for surface roughness scale z_0.

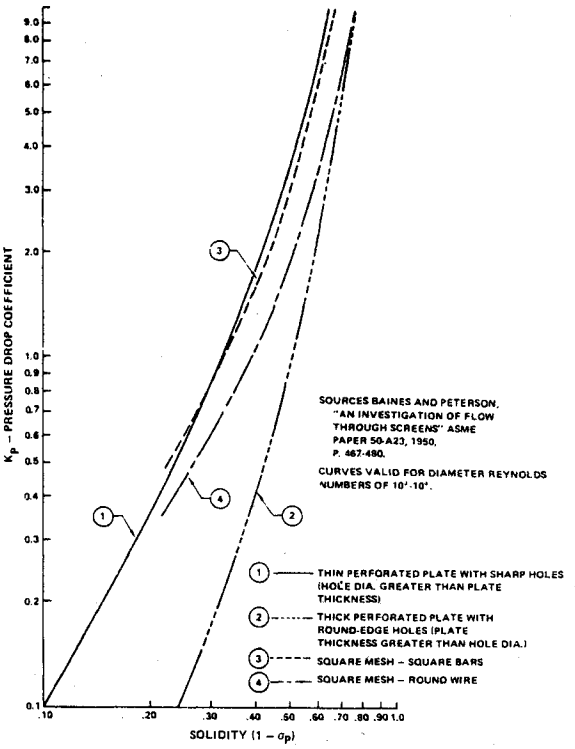

Fig. 9 Pressure loss coefficient as a function of solidity.

Steady Distortion Design

29) Determine maximum azimuthal velocity in vortex, U_{2A} (to be estimated by inflow control structure designer for particular test stand under consideration).

30) Compute maximum value of flow angle ratio product, $\alpha_p \alpha_H$,

$$\alpha_p \alpha_H = \sqrt{\overline{u_{AF}^2}} / U_{2A}$$

31) Determine maximum precontraction streamwise velocity deficit, ΔU_{1A} (to be estimated by inflow control structure designer for particular test stand under consideration).

32) Solve the equation for the perforated plate (gauze) flow angle ratio, α_p,

$$\frac{2\alpha_p^3 + \alpha_p^2 - 1.21\alpha_p}{\alpha_p^3 + 1.21} = \frac{\sqrt{\overline{u_{AF}^2}}}{\Delta U_{1A}} l_{IS} \times \left\{ \frac{\alpha_p + \alpha_p \alpha_H - 0.201 Re^{-1/4} \alpha_p [\ln \alpha_p \alpha_H - \ln \alpha_p]}{\alpha_p + \alpha_p \alpha_H (1 + 0.201 Re^{-1/4} [\ln \alpha_p \alpha_H - \ln \alpha_p])} \right\}$$

33) Compute resistance of perforated plate (gauze), K_p,

$$K_p = 1.21 \alpha_p^{-2} - 1$$

34) Compute flow angle ratio of honeycomb, α_H,

$$\alpha_H = \alpha_p \alpha_H / \alpha_p$$

35) Compute resistance of honeycomb, K_H,

$$K_H = -0.201 Re^{1/4} \ln \alpha_H$$

Conservative Design

36) Compare resistance of perforated plate (gauze) for atmospheric turbulence and steady distortion designs (items 26 and 33). Choose the larger, K_p.

37) Compare flow angle ratio of honeycomb for atmospheric turbulence and steady distortion designs (items 27 and 34). Choose the smaller, α_H.

38) Compute honeycomb length to diameter ratio, l/d,

$$l/d = -(1/\pi) \ln \alpha_H$$

39) Determine perforated plate open area ratio from Fig. 9, σ_p.

40) Determine the maximum Mach number of flow incident on the inflow control structure, M_{ICS}.

41) Plot perforated plate thickness, l_p, against hole diameter, d_p, using the transmission loss criterion of less than 1 dB in the 24th one-third octave band.

$$l_p = 5.39 \cdot 10^{-3} [5.04 - (2 + K_p M_{ICS})^2]^{1/2} \sigma_p - (1 - \sigma_p) d_p$$

42) Select a perforated plate thickness and hole diameter consistent with the estimate of d_{ICS} in item 10.

Conclusions, Results, and Recommendations

1) Use of an inflow control structure during static testing of a JT9D engine is shown to significantly reduce blade passage frequency tones but to have a small effect on twice blade passage frequency tones.

2) Use of an inflow control structure with a JT9D engine is shown to significantly improve agreement between static data projected to flight and flight data for the blade passage frequency fan tone.

3) A design system is presented that prescribes inflow control structure shape, size, and detailed construction.

4) Further assessment of inflow control structure effectiveness by comparing static data projected to flight with flight data should be carried out for other engine types.

5) Further assessment and improvement of the static to flight projection methodology should be carried out.

Acknowledgments

The work summarized herein was performed by the Pratt and Whitney Aircraft Group, Commercial Products Division, and the Boeing Commercial Airplane Company under contract from the National Aeronautics and Space Administration Langley Research Center (NAS1-15085). Contributions from U. Ganz, of the Boeing Commercial Airplane Company and M. Gedge, K. Robbins, and R. Larson of the Pratt and Whitney Commercial Products Division are acknowledged.

References

[1] Peracchio, A.A., Ganz, U.W., et al., "Studies on Proper Simulation During Static Testing of Forward Speed Effects on Fan Noise," NASA CR 165626, Sept. 1980.

[2] Atvars, Y. and Rogers, D.F. "The Development of Inflow Control Devices for Improved Simulation of Flight Noise Levels During Static Testing of a HBPR Turbofan Engine," AIAA Paper 80-1024, June 1980.

[3] Rodgers, D.F. and Ganz, U.W., "Aerodynamic Assessment of Methods to Simulate Flight Inflow Characteristics During Static Engine Testing," AIAA Paper 80-1023, June 1980.

[4] Ganz, U.W. "Analytical Investigation of Fan Tone Noise Due to Ingested Atmospheric Turbulence," Phase I Final Report, NASA Contract NAS1-15085, NASA CR-3302, Aug. 1980.

[5] Gedge, M.R., "A Design Procedure for Fan Inflow Control Structures," Phase II Final Report, NASA Contract NAS1-15085, NASA CR-165625, Sept. 1980.